Biomedical Signal Processing and Control 81 (2023) 104480

Contents lists available at ScienceDirect

Biomedical Signal Processing and Control

journal homepage: www.elsevier.com/locate/bspc

An EMG-driven musculoskeletal model for estimation of wrist kinematics using mirrored bilateral movement

Yihui Zhao, Zhenhong Li, Zhiqiang Zhang, Kun Qian, Shengquan Xie *

University of Leeds, Woodhouse Lane, Leeds, LS2 9JT, United Kingdom

ARTICLE INFO

Keywords:
Musculoskeletal model
Electromyogram signal
Mirrored bilateral movement
Myoelectric control

ABSTRACT

Myoelectric control methods aim at driving electric prostheses in restoring functionality in daily life for amputees. To achieve the simultaneous and proportional estimation of multiple kinematics of the wrist joint, model-free approaches are broadly developed but rely on the abundant training data and the numerical functions that omit neuro-mechanical transformation. The musculoskeletal model-based approach entails the underlying muscular transformation from neuro-commands to the limb motion. However, the model-based approach for simultaneous kinematics estimation of the distal joint, i.e., wrist joint, is often overlooked. This paper proposes an electromyography (EMG)-driven musculoskeletal model to estimate the wrist joint kinematics involving wrist flexion/extension and radial/ulnar deviation. The proposed approach computes the internal force/joint torque and integrates the wrist kinematics using the forward dynamics. The mirrored bilateral movements are utilised to optimise the internal physiological parameters, which improve the feasibility for the practical application of myoelectric control for the unilateral transradial amputee. Experiments are conducted on six able-bodied subjects, involving a series of wrist movements in free space. Results demonstrate the proposed model-based approach provides high estimation accuracy in the contralateral case with mean coefficient of determination of 0.86 and 0.82 for wrist flexion/extension and radial/ulnar deviation, respectively. The proposed approach and setup give reliable and feasible meaning for the simultaneous and proportional control of multiple wrist kinematics.

1. Introduction

The loss of upper limbs impairs physical functionality and mobility that degrades the quality of life significantly. The myoelectric control methods, using the surface electromyogram (EMG) from the residual limb, strive to restore functionalities for amputees to perform the activities of daily life [1]. A conventional approach to estimate the joint kinematics using the EMG signal is concerned with the pattern recognition algorithm [2]. This algorithm is limited by its inherent sequential control strategy, which recognises the desired motion classes at a time [3]. To realise the natural movements of the wrist joint that involve the combined activation of the multiple degrees-of-freedom (DoFs), the proportional control needs to be achieved [4,5]. That is, continuous kinematic variables are derived from the EMG signal, instead of desired motion classes [6]. Furthermore, myoelectric control methods should provide the proportional control of multiple DoFs simultaneously [7].

The techniques for simultaneous and proportional kinematics estimation can be categorised into the model-free approach and the musculoskeletal (MSK) model. The model-free approaches establish relationships between EMG signals and desired movements using numerical functions [8–10]. For example, Lei et al. utilised the BP network to estimate the continuous elbow motion.[11]. Zhang et al. employed the Gaussian regression algorithm to achieve the simultaneous control of a robotic hand. Moreover, Bao et al. proposed the deep learning algorithm to achieve the wrist kinematics estimation [12]. The model-free approaches are limited by the demand for abundant data to train the relevant transfer functions. The trained functions underlying one specific condition, may not be able to respond to a novel condition, i.e., different postures or loading conditions [13,14].

The model-based approach is an alternative approach for motion estimation which comprises muscle physiology, i.e., Hill's muscle model, and musculoskeletal geometry to mimic the physiological human movement. This approach entails the underlying muscular transformation from neural commands to the corresponding limb motion. Recently, the model-based approach has emerged for the proportional estimation about the single DoF. For instance, Sheng et al. proposed an EMG-driven MSK model to estimate joint angle trajectory of an elbow isokinetic exercise [15]. Han et al. also utilised the model-based approach in

* Corresponding author.
E-mail address: S.Q.Xie@leeds.ac.uk (S. Xie).

https://doi.org/10.1016/j.bspc.2022.104480
Received 8 May 2022; Received in revised form 14 October 2022; Accepted 27 November 2022
Available online 14 December 2022

conjunction with EMG features to estimate the elbow flexion/extension movements [16]. To provide the myoelectric control simultaneously, Blana et al. proposed the MSK model for myoelectric control of hand movements to perform the American sign language [17]. Nevertheless, this model is based on the simulated EMG signals. Pan et al. proposed a generic MSK model to estimate the wrist and metacarpophalangeal (MCP) joint flexion/extension under the different loading conditions [18]. However, only wrist flexion/extension motion are concerned in their model. The wrist primary muscles also contribute to ulnar/radial deviation.

The physiological parameters in the model-based approach need to be optimised to each individual to preserve the estimation accuracy. However, the training data, which requires the recording of the EMG signal and the corresponding wrist motion from the same side, is not possible to be obtained directly from the amputees. Studies addressed this problem by the mirrored bilateral movement training strategy because the amputees are able to generate the virtual movements voluntarily with their amputated side [19,20]. The similar neural muscular contractions have been observed during the mirrored bilateral movement [21]. In [18], the MSK model was developed for amputees through the mirrored bilateral movement. However, only two wrist muscles are included and the optimised parameters exceeded the physiological range, e.g., the optimised muscle fibre length exceeds the physiological measurement in *vivo* [22].

In the present study, an EMG-driven MSK model is developed to estimate two DoFs wrist motions using the mirrored bilateral movement training strategy. We ask the human subjects to perform a series of mirrored bilateral wrist movements in free space. We then optimise the physiological parameters under the contralateral cases, i.e., EMG signals are recorded from one limb and the wrist kinematic data are recorded from the contralateral limb, and compare the estimation performance with the ipsilateral cases which EMG signals and kinematic data are recorded from the same side of the limb. We hypothesised that there is no statistical differences between the contralateral cases and the ipsilateral cases. The main contributions of the present study include: (1) the feasibility of the EMG-driven MSK model to estimate the wrist motion under the contralateral cases is demonstrated; (2) the reliability for estimation of wrist multiple kinematics via the EMG-driven MSK model is evaluated; (3) the outcomes demonstrate the potential of the EMG-driven MSK model for the simultaneous and proportional control of multiple wrist kinematics.

2. Methods

2.1. Experimental protocol

Six able-bodied subjects participant in the experiments (referenced as S1–S6, the ages between 25 and 31). The experimental information sheets are given to all subjects and the consent forms are signed prior to the experiment. The experimental protocol is approved by Maths and Physical Science and Engineering Joint Faculty Research Ethics Committee of the University of Leeds (MEEC 18-002).

At the start of the experiments, the subjects are asked to sit on an armchair with the torso fully straight, the shoulders are abducted around 30° and the elbows are flexed about 90°. The elbows are supported by two customised armrests and the forearms and MCP joints are kept relaxed. To ensure the symmetric position of the upper limbs is achieved, the wrist movements are computed and displayed on a PC screen. The neutral position of the wrist joint is defined as the palm facing inwards. Surface EMG signals from the right forearm and the motion data from both forearms are recorded during the experiments. A period of time is given for the subject to familiarise with the experimental protocol before the experiment and the maximum voluntary contractions (MVC) are recorded.

Subjects are instructed to perform a series of mirrored bilateral movements, involving the one DOF and the combination of two DoFs movements. As shown in Table 1, the experimental trials consist of purely wrist flexion/extension, radial/ulnar deviation, and the combinations (clockwise and anticlockwise rotations). Subjects are instructed to perform five repetitions of each movement set in one trial with the frequency of approximately 0.5 Hz for one repetition, and five trials are recorded for each movement set. To optimise the parameter in the EMG-driven MSK model, one trial from each movement set, which includes the EMG data for the right limb and bilateral wrist motion, is selected as the calibration trial. This enables parameter optimisation for both ipsilateral case and contralateral case. The rest four trials under the same movement set are then used to evaluate and compare the estimation performance between the ipsilateral case and contralateral case. A five-minute break is given between trials to prevent muscle fatigue.

Table 1
Experimental protocol.

Index	Movement set	Active DoF(s)
1	Sinusoidal movement	Wrist flexion/extension (WFE)
2	Sinusoidal movement	Radial/Ulnar Deviation (RUD)
3	Combined movement in a circular clockwise (CW)/Counterclockwise (CCW)	WFE and RUD

2.2. Data acquisition

2.2.1. EMG recording

The surface EMG signals are recorded by the Avanti Sensors (Delsys Trigno^{TM}) in this experiment. The EMG signals of five muscles ($i = 1, 2, \ldots, 5$) articulating the wrist joint are collected, including Flexor Carpi Radialis (FCR), Flexor Carpi Ulnaris (FCU), Extensor Carpi Radialis Longus (ECRL), Extensor Carpi Radialis Brevis (ECRB) and Extensor Carpi Ulnaris (ECU). EMG signals are recorded from the right forearm (right top corner in Fig. 1). The location of electrode placement are found by palpation and evaluated by performing contraction while looking at the signal prior to experiment. The skin is cleaned using an alcohol wipe to minimise the impedance prior to electrode placement (shaved if necessary). The EMG signals are acquired through the base station, sampled at 2000 Hz.

2.2.2. Wrist motion recording

The wrist kinematics data are captured using a 8-camera motion capture system (VICON Motion Systems Ltd. UK). To compute the wrist flexion/extension angle and ulnar/radial deviation angle, a coordinated system is adopted based on [23]. The reflective markers are attached symmetrically on the subject's forearms (seven markers at each limb). Four markers are allocated in hand area, including the radial head of the second metacarpal bone (RMC), the ulnar head of the fifth metacarpal bone (UMC), the radial styloid (STR) and the ulnar styloid (STU). Two markers are placed over the lateral (MEP) and medial epicondyles (LEP) of the humerus. Two markers are positioned on the acromio-clavicular join (SHO) and three markers are attached on the 7th spinous process (C7), right clavicle (CLAV) and xiphoid (STE) respectively. The qualities of the movements data are evaluated after each trial, trials containing the markers' trajectory with the excessive gaps are abandoned. The kinematic data are sampled at 250 Hz and low-pass filtered.

2.3. Data processing

2.3.1. EMG processing

The recorded EMG signals are filtered using a 4th order Butterworth band-pass filter (pass band at 20 Hz and 450 Hz) to remove the movement artefact and dc offset. The filtered signals are fully rectified and

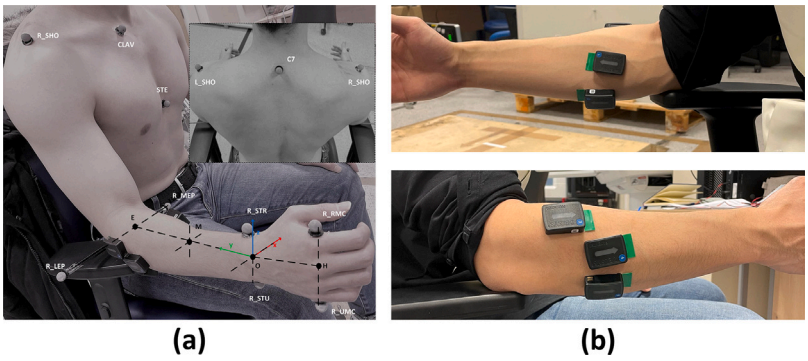

Fig. 1. (a) Markers' position of the right limb and the coordinate system for wrist kinematics calculation. Three markers are attached on torso, including the 7th spinous process (C7), right clavicle (CLAV) and xiphoid (STE). Markers on the left limb are attached symmetrically. (b) Electrodes are attached over the wrist primary muscles.

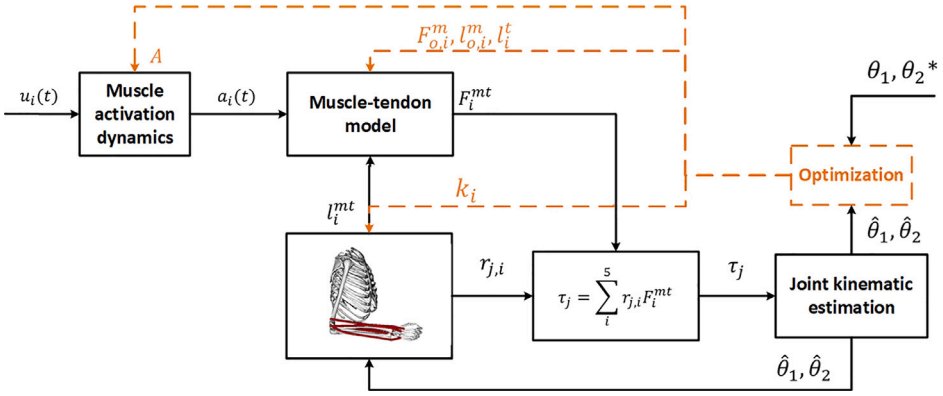

Fig. 2. The flowchart of the EMG-driven MSK model for estimation wrist joint kinematics. Muscle activation dynamics transforms the $u_i(t)$ to $a_i(t)$, and muscle–tendon model produces the muscle–tendon force F_i^{mt}. The estimated joint motion $\hat{\theta}_1$, $\hat{\theta}_2$ are computed through the joint kinematic estimation model. Orange dash line denotes the parameter optimisation, which aims to determine the subject-specific parameters for each subject. Note that the measured joint angles from the same side of the recorded EMG signal indicates the ipsilateral case, and the measure joint angles from the opposite side denotes the contralateral case.

low-pass filtered by a 4th order Butterworth low-pass filter at a corner frequency of 4 Hz. To interpret the envelope of the muscles activities between 0 and 1, the filtered signals are normalised by the MVCs, resulting in enveloped signals $u_i(t)$.

2.3.2. Kinematics data processing

Similar to [23], the coordinate system (Fig. 1(a)) can be described in the following. The original point **O** is defined as the centre of the wrist, at the midpoint between the STR and STU. The y-axis is located along with the centre axis of the forearm, the positive direction points to the proximal joint. The x-axis is perpendicular to the palm, the positive direction points inward. Then the z-axis is determined by the right-hand rule, orthogonal to the y-axis and x-axis. The positive direction points upward. The midpoint between the RMC and UMC is denoted by H, allocating on the y-z plane. Thus the wrist joint angles θ_j $(j = 1, 2)$ for wrist flexion/extension and radial/ulnar deviation can be calculated by the following equations.

$$\theta_1 = \arctan(\frac{H_x}{H_y}) \tag{1}$$

$$\theta_2 = \arctan(\frac{H_z}{H_y}) \tag{2}$$

where H_x, H_y and H_z are the projections of H on x-axis, y-axis and z-axis respectively. θ_1 and θ_2 represent the wrist flexion/extension and radial/ulnar deviation respectively. The positive directions correspond to the wrist flexion and ulnar deviation respectively. The surface EMG signals and kinematic data are synchronised in VICON Nexus software through a trigger module. The synchronised and processed signals are resampled to 100 Hz for computing the muscle activation levels [13].

2.4. Musculoskeletal model-based approach

Fig. 2 gives the flowchart of the proposed musculoskeletal model-based approach for wrist joint motion estimation, which comprises the muscle activation dynamics, the muscle–tendon model, and the joint kinematics estimation model. The muscle activation dynamics computes the muscle activation levels of the wrist muscles. Then the muscle force are calculated in response to muscle activation level and current states of muscle-fibre length. The joint angles are estimated with the combination of the skeletal properties through the forward dynamics.

2.4.1. Muscle activation dynamics

To account for the non-linearity between the enveloped signal $u_i(t)$ and muscle activation $a_i(t)$, muscle activation dynamics is used, according to [24]:

$$a_i(t) = \frac{e^{Au_i(t)} - 1}{e^A - 1} \tag{3}$$

where A is the non-linear shape factor.

2.4.2. Muscle-tendon model

For each muscle, the muscle–tendon model is modelled as an elastic tendon connected in series with a muscle fibre (Hill's muscle model). The muscle fibre contains the contractile element (CE) in parallel with passive element (PE). In this paper, the tendon is assumed as a rigid element, thus the muscle–tendon force F_i^{mt} produced by the muscle–tendon model is computed as [24]:

$$F_i^{mt} = \left(F_{CE,i} + F_{PE,i}\right)\cos\phi_i \tag{4}$$

where $F_{CE,i}$, and $F_{PE,i}$ denotes the force generated by CE and PE, respectively. ϕ_i is pennation angle between the tendon and muscle fibre, which can be obtained by:

$$\phi_i = \sin^{-1}\left(\frac{l^m_{o,i}\sin\phi_{o,i}}{l^m_i}\right) \tag{5}$$

in which $\phi_{o,i}$ represents the optimal pennation angle. $l^m_{o,i}$ and l^m_i are the optimal muscle fibre length and muscle fibre length, respectively.

The active force generated by CE is the function of the muscle active level $a_i(t)$ and maximum isometric force $F^m_{o,i}$, which is written as:

$$F_{CE,i} = F^m_{o,i} f_a(\bar{l}^m_{i,a}) f(\bar{v}_i) a_i(t) \tag{6}$$

where $f_a(\bar{l}^m_{i,a})$ and $f(\bar{v}_i)$ are the active force–length relationship and the force–velocity relationship respectively. $\bar{l}^m_{i,a}$ is equal to $\bar{l}^m_{i,a} = l^m_i/(l^m_{o,i}(\lambda(1-a_i(t))+1))$, and λ is set to 0.15 in this study [25]. $\bar{v}_i$ is the normalisation of muscle contraction velocity v_i to the maximum contraction velocity, which is set to 10 $l^m_{o,i}$/ sec. v_i is the derivative of the muscle fibre length with respect to time. The $f_a(\bar{l}^m_{i,a})$ and $f(\bar{v}_i)$ are given as:

$$f_a(\bar{l}^m_{i,a}) = e^{-(\bar{l}^m_{i,a}-1)^2 k_0^{-1}} \tag{7}$$

$$f(\bar{v}_i) = \begin{cases} \frac{0.3(\bar{v}_i+1)}{-\bar{v}_i+0.3} & \bar{v}_i \le 0 \\ \frac{2.34\bar{v}_i+0.039}{1.3\bar{v}_i+0.039} & \bar{v}_i > 0 \end{cases} \tag{8}$$

where k_0 is set to 0.45 in order to approximate the force–length relationship.

The force $F_{PE,i}$ is the passive force generated by the PE in muscle fibre, which is calculated as:

$$F_{PE,i} = F^m_{o,i} f_p(\bar{l}^m_i) \tag{9}$$

where l^m_i is the normalisation of muscle fibre length with respect to $l^m_{o,i}$. $f_p(\bar{l}^m_i)$ denotes passive force–length function when the muscle fibre length exceeds the optimal muscle fibre length [26]:

$$f_p(\bar{l}^m_i) = \frac{e^{10(\bar{l}^m_i-1)}}{e^5} \tag{10}$$

In order to obtain the current states of the muscle fibre length, a large combinations of wrist movement involving wrist flexion/extension and radial/ulnar deviation simultaneously are simulated by restricting other DoFs to the experimental posture [27]. The simulated results are exported to generate the regression equation of the muscle–tendon lengths l^{mt}_i with respect to the wrist joint angles. Then the muscle fibre length can be obtained by:

$$l^m_i = \sqrt{(l^m_{o,i}\sin\phi_{o,i})^2 + (k_i l^{mt}_i - l^t_i)^2} \tag{11}$$

where l^{mt}_i and l^t_i are the muscle–tendon length and tendon length respectively. The scale coefficient k_i is introduced to account for the difference of the muscle–tendon length across subjects. The moment arm is then obtained by the partial derivatives of the muscle–tendon length with respect to the corresponding joint angles:

$$r_{j,i} = \frac{\partial l^{mt}_i}{\partial \theta_j} \tag{12}$$

where $r_{j,i}$ represents the moment arm of ith muscle with respect to the jth joint angle. Therefore, the corresponding wrist joint torques can be computed by:

$$\tau_j = \sum_{i=1}^{5} r_{j,i} F^{mt}_i \tag{13}$$

where τ_j is a 2 × 1 vector, representing the joint torques at wrist flexion/extension and ulnar/radial deviation respectively.

2.4.3. Joint kinematics estimation model

To obtain the wrist kinematics in both flexion/extension and radial/ulnar deviation, the wrist joint is modelled as a universal joint. The distance between the axes of two DoFs is neglected in this study, due to the negligible effects on the wrist dynamics [28]. The wrist kinematics are then calculated by:

$$\tau_j = M\ddot{\theta}_j + C\dot{\theta}_j + K\theta_j + G \tag{14}$$

where τ_j denotes the computed joint torque. Matrix M denotes a symmetric matrix that represents the inertia term, in which the inertia of both axes is estimated based on the subject's weight and height [29]. The symmetric matrix C denotes the damping parameters to mimic the biological joint damping, which are set to 0.3 Nms/rad and 0.6 Nms/rad for θ_1 and θ_2 respectively. The matrix K are the passive stiffness coefficients for the wrist joint, which are assigned to mean value in [30]. G is the gravitational effects on radial/ulnar deviation which is equal to $mgl\cos(\theta_2)$, m, g, and l are the hand mass, gravitational constant, the length between the wrist joint to the third metacarpal. $\ddot{\theta}_j$, $\dot{\theta}_j$ and θ_j are the joint accelerations, joint velocities and joint angles respectively. As shown in Fig. 2, the computed joint accelerations are forward integrated to estimate the next state of wrist joint angles through the 4th order Runge–Kutta method.

2.4.4. Parameters optimisation

The proposed model-based approach contains several physiological parameters that account for the difference of the muscle property across subjects, including the non-linear shape factor A, the maximum isometric muscle force $F^m_{o,i}$, optimal muscle fibre length $l^m_{o,i}$, tendon length l^t_i and scale coefficient k_i. The parameter optimisation problem is solved by minimising the difference of the estimation and measurement through optimisation trials (orange lines in Fig. 2). The objective function is written as:

$$\chi = [F^m_{o,i}, l^m_{o,i}, l^t_i, k_i, A]^T \tag{15}$$

$$\hat{\chi} = \arg\min_{\chi}\{f(\chi)\} \tag{16}$$

where

$$f(\chi) = \frac{1}{N}\sum_{j=1}^{2}\sum_{n=1}^{N}(\theta_j - \hat{\theta}_j) \tag{17}$$

where $f(\chi)$ is the objective function that minimises the difference between the estimated joint angles and measured joint angles. θ_j and $\hat{\theta}_j$ are the measured joint angles and estimated joint angles respectively. N is the number of samples. Genetic algorithm in MATLAB optimisation toolbox is used in this study. Table 2 gives the nominal value of the physiological parameters, according to [27]. The $F^m_{o,i}$, $l^m_{o,i}$, and l^t_i are constrained within ±50%, ±5%, and ±5% of them nominal value respectively. The A is constrained between 0.001 and 3, based on [26]. k_i is constrained between 0.9 and 1.2.

The sensitivity analysis is conducted to qualify the effects of the physiological parameters. According to [31], the sensitivity of each parameter is calculated as:

$$SI_j = \frac{(M_{j,pret} - M_{opt})/M_{opt}}{(P_{j,pret} - P_{j,opt})/P_{j,opt}} \tag{18}$$

where $M_{j,pret}$ and M_{opt} denote the perturbed model output and optimal model output respectively. $P_{j,pert}$ and $P_{j,opt}$ are the jth perturbed parameter and the jth baseline parameter in the proposed model respectively. The maximum isometric forces are perturbed by ±20% and other parameters are perturbed by ±10%. The sensitivity coefficient SI_j is used for comparison between parameters.

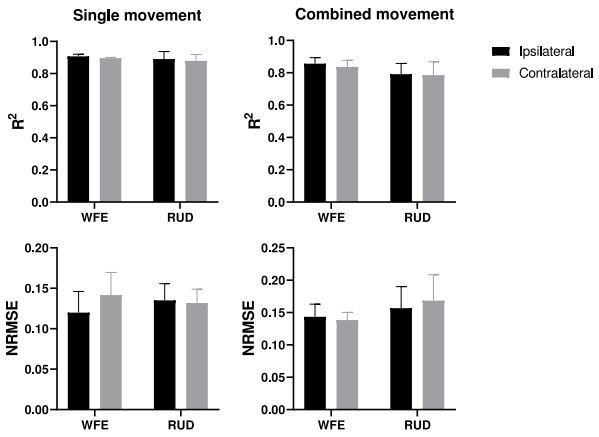

Fig. 3. Comparison of the estimation performance between the ipsilateral and contralateral case in the single movement and combined movement trials. Top panel and bottom panel present the R^2 and NRMSE respectively. WFE and RUD correspond to the wrist flexion/extension and radial/ulnar deviation respectively.

Table 2
Nominal value of the physiological parameters.

Parameters (units)	FCR	FCU	ECRL	ECRB	ECU
$F^m_{o,i}$ (N)	407	479	337	252	192
$l^m_{o,i}$ (m)	0.062	0.051	0.081	0.058	0.062
l^t_i (m)	0.24	0.26	0.24	0.22	0.2285
$\phi_{o,i}$ (rad)	0.05	0.2	0	0.16	0.06
k_i	1	1	1	1	1

2.5. Performance index

To quantify the estimation performance of the proposed EMG-driven model, the coefficient of determination (R^2) and normalised root-mean-square-error (NRMSE) are used as the metric for each DoF, which can be expressed as

$$R^2_j = 1 - \frac{\mathrm{Var}(\theta_j - \hat{\theta}_j)}{\mathrm{Var}(\theta_j)} \tag{19}$$

$$\mathrm{NRMSE_j} = \frac{\sqrt{\frac{1}{N}\sum_{n=1}^{N}(\theta_{j,n} - \hat{\theta}_{j,n})^2}}{\theta_{max,j} - \theta_{min,j}} \tag{20}$$

where θ_j and $\hat{\theta}_j$ represent the jth measured joint angle and the jth estimated joint angle respectively. $\theta_{max,j}$ and $\theta_{min,j}$ are the maximum and minimum value of the jth measured joint angle. In Eq. (19), the numerator represents the mean-square-error (MSE) and denominator is the total variance [32]. The NRMSE and R^2 quantify the difference in terms of amplitude and correlation between the estimated joint angles and the measured joint angles. Higher values of R^2 and lower NRMSE indicate the model-based approach can estimate the joint angle accurately. In addition, separate one-way ANOVAs are conducted for each DoF to evaluate the differences between the ipsilateral case and contralateral case in terms of the R^2 and NRMSE. Statistical significance value is set to $p = 0.05$.

3. Results

For each subject, the wrist kinematic data are collected bilaterally and the EMG signal is collected from the dominant side are used to calibrate the muscle–tendon parameters. The estimated results for the ipsilateral case and contralateral case across the single DoF movement and combined movement trials are illustrated in Fig. 3. The one-way ANOVA analysis indicates that there is no statistical difference between the ipsilateral case and the contralateral case. The p values are 0.27 and 0.77 for wrist flexion/extension (WFE) and radial/ulnar deviation (RUD) respectively. In the single activation trial, the mean R^2 and mean NRMSE in the case of ipsi(contra)lateral are: 0.905(0.895), 0.118(0.141); 0.887(0.875), 0.138(0.131) for the WFE and RUD respectively. In the combined motion trials, mean R^2 and mean NRMSE are 0.856 (0.838) and 0.143 (0.138) for WFE. For the RUD, the mean R^2 and mean NRMSE are 0.791 (0.784) and 0.157 (0.176).

Table 3
Estimation performance (mean R^2 and mean NRMSE) across all subjects in the contralateral case.

Subject	Movement set	R^2		NRMSE	
		WFE	RUD	WFE	RUD
S1	T1/T2	0.90	0.85	0.14	0.14
	T3	0.79	0.85	0.14	0.17
	T4	0.81	0.80	0.13	0.14
S2	T1/T2	0.90	0.90	0.11	0.11
	T3	0.84	0.85	0.14	0.12
	T4	0.88	0.82	0.12	0.16
S3	T1/T2	0.89	0.92	0.18	0.12
	T3	0.93	0.57	0.12	0.16
	T4	0.86	0.78	0.15	0.26
S4	T1/T2	0.89	0.89	0.17	0.13
	T3	0.79	0.74	0.13	0.18
	T4	0.85	0.73	0.15	0.23
S5	T1/T2	0.90	0.90	0.12	0.13
	T3	0.83	0.88	0.14	0.13
	T4	0.80	0.84	0.14	0.15
S6	T1/T2	0.89	0.81	0.13	0.16
	T3	0.83	0.81	0.16	0.17
	T4	0.83	0.75	0.14	0.15
Mean		0.86	0.82	0.14	0.16
Std.		0.04	0.08	0.02	0.04

Std. = standard deviation.

The estimation performance of the contralateral case are summarised in Table 3, in terms of the R^2 and NRMSE for each subject. Note that for the first two movement sets, the performance criteria is only calculated for the primary DoF, i.e., WFE for movement T1 and RUD for T2. Results indicate the proposed EMG-driven MSK model can provide an accurate wrist joint kinematics estimation. When one DoF is activated, the estimation performance is better than the performance when the combined movements are performed, e.g., S1 in the contralateral case, the R^2 of WFE is 0.90 in the single movement trial and is around 0.80 in the combined trial. One additional representative example of the contralateral case is given in Fig. 4. In addition, Fig. 6 depicts the representative example of the comparison between the ipsilateral and contralateral cases.

The results of the sensitivity analysis are shown in Fig. 5. The scale factor and muscle tendon length have large sensitivities in the EMG-driven muscle model. The optimal muscle fibre length and maximum isometric force have the moderate influences on the model output. According to Eq. (11), the scale coefficient and muscle tendon length are used to determine the current state of the muscle fibre length, which affects active force generating capacities significantly, i.e., the active force–length relationship.

4. Discussion

4.1. Mirrored bilateral movement

This study proposes the EMG-driven MSK model to estimate the multiple DoF wrist kinematics of the contralateral side using the EMG signals captured from the ipsilateral side. The mirrored bilateral movements train strategy is conducted to collect the EMG and kinematic data for the subject-specific parameter optimisation. This can be achieved by two important factors. It has been shown that the amputees can

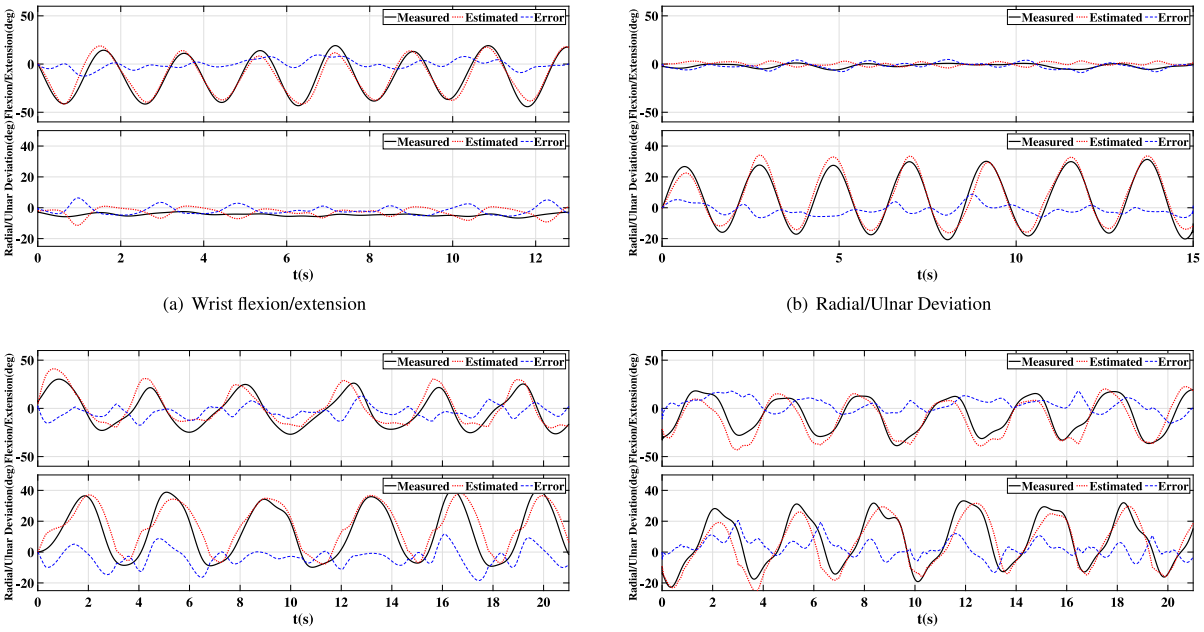

(a) Wrist flexion/extension (b) Radial/Ulnar Deviation

(c) Clockwise trial (d) Counter-clockwise trial

Fig. 4. Estimation performance of the representative subject for all trials in the contralateral case. The R^2 and NRMSE for the corresponding trials are: (a) 0.95 (0.07) for WFE, (b) 0.96 (0.08) for RUD, (c) 0.84 (0.10) for WFE and 0.87 (0.11) for RUD and (d) 0.86 (0.12) for WFE and 0.89 (0.10) for RUD. Errors are presented in blue dashed line.

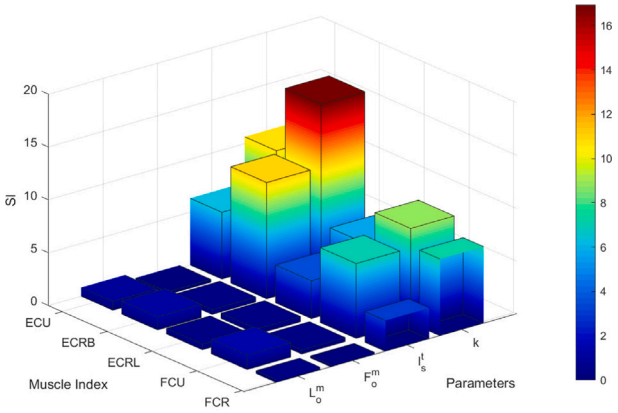

Fig. 5. Sensitivity analysis of the physiological parameters.

voluntarily produce the muscle activities to experience different movements after amputations which suggests that the phantom arm remains the functionalities of expressing the preserved limb movements by generating relevant motor commands as if the limb is still there [33]. Furthermore, it is found that similar neural muscular commands can be produced during the mirrored bilateral movements [21]. For example, Zhang et al. applied the mirrored bilateral movement to collect the training data for the myoelectic control of a robotic hand [34]. Moreover, Jiang et al. demonstrated the mirrored bilateral movement training strategy on trans radial amputees to estimate the wrist motion [23]. Thus, the EMG signals from amputees can be applied to the proposed model-based approach to obtain the subject-specific parameters. The present shows the feasibility of the EMG-driven MSK model for future research on amputees. Future studies will be carried out to extend the EMG-driven MKS model for amputees.

The experimental results demonstrate that the feasibility of the proposed model-based approach to estimate the wrist joint angles of contralateral side by using the EMG signals from ipsilateral side using the mirrored bilateral movements. This approach provides the accurate joint angular movements estimation in the contralateral case (Fig. 3), which can be replicated for the unilateral amputees. The model-based approach requires the parameters to be optimised by the objective function (equation (17)) and the training data. The mirrored bilateral movement training strategy, therefore, provides a solution for the proposed approach to facilitate the parameter optimisation, in which the kinematic data are unavailable from amputated side.

4.2. Model performance

The experimental results demonstrate that the proposed EMG-driven model can respond to the able-bodied subject's intention in the simultaneous and proportional wrist joint movements. It reflects the biological process from the EMG signals to the wrist kinematics, interpreting the internal muscle active/passive force and the joint torques [13]. In the contralateral cases, the mean R^2 are 0.86 ($\pm$0.04) and 0.82 ($\pm$0.08) for WFE and RUD respectively, which is slightly lower than the ipsilateral case. Both cases have the similar NRMSE, which are 0.14 ($\pm$0.02) and 0.16 ($\pm$0.04) for ipsi and contralateral cases respectively.

For the single DoF movement trials, the estimation performance shows a high correlation and lower NRMSE than the combined movement trials. One potential issue is that the performance is affected by the noise of the signal, which leads to the model treats the crosstalk signals as the muscle activities and generates the muscle force. Moreover, the passive tendon force is another issue that results in estimation errors. Besides, the subject may slightly involve the forearm pronation/supination when the combined movements are performed, which the muscle activities may deviate. The primary wrist muscles are selected in this study. For the single DoF movements, the selected wrist muscles act as the antagonist and agonist pair. For example, the FCR and FCU are the flexor group and activated simultaneously. These muscles are active alone when both DoFs are actuated [35,36]. For the amputees, it may be difficult to locate the targeted muscles after amputation. Some studies applied the High-density (HD) EMG electrodes to record the muscle activities from the amputated side [23,37]. Therefore, the activities of the targeted muscles of the missing limb can be clustered and identified by the spatial information [35,38], and estimated through the muscle synergy technique [39].

State-of-the-art myoelectric control schemes are mostly based on machine learning techniques, extracting features from the captured

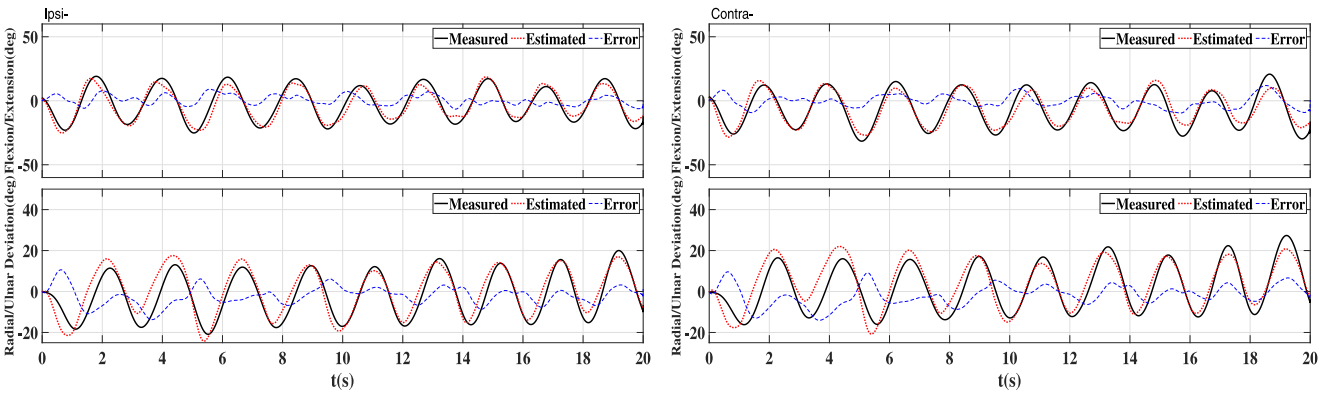

Fig. 6. Representative example for comparison between the ipsilateral case (left) and contralateral case (right). Red dash line denotes the estimated WFE angles (top figures) and RUD angles (bottom figures), black line denote the measured joint angles. For ipsilateral case, the R^2 (NRMSE) are 0.91 (0.08) for WFE and 0.85 (0.12) for RUD, respectively. For contralateral case, the R^2 (NRMSE) are 0.89 (0.09) and 0.82 (0.12) for WFE and RUD respectively. Errors are presented in blue dashed line.

EMG signals, training the numerical transfer functions, and then to estimate the joint angles correspondingly [37]. Although it cannot be compared with data-driven approaches, the estimation performance shows similar performance compared with the model-free approaches in terms of R^2. Muceli et al. reported that the overall R^2 for all DoFs has over 0.79 [37]. Jiang *el al.* showed higher R^2 in wrist flexion/extension and radial/ulnar deviation movement when only DoF was close to the maximum range of motion (mean R^2 = 0.88 for contralateral case) [23]. However, machine learning techniques requires abundant datasets to maximise the estimation performance. Furthermore, it is proved that the musculoskeletal model-based approach is robust to the different postures. Pan et al. reported that for the same training data, the model-based approach is significantly better performance than the artificial neural network (ANN) and linear regression (LR) algorithm [13]. This is may due to the 'over-fitting' problem in the model-free approach. In [36], a regression model combined with a generic musculoskeletal model was proposed to estimate the multiple wrist joint kinematics. It should be noted that the effects of forearm pronation/supination on the wrist flexion/extension and radial/ulnar deviation are excluded in their study. The proposed model shows the similar R^2 compared with their study (0.84 vs. 0.8 for able-bodied subjects) without increasing computational complexity.

The proposed model-based approach contains several physiological parameters, which affect the model output significantly, i.e., isometric maximum force, muscle fibre length, tendon length and non-linear shape factor. The pennation angle is set to constant due to the fact it has minor effect on the model output [40]. These parameters cannot be obtained from amputees. Nevertheless, the proposed model can be established for the phantom arm using the mirrored bilateral movement training strategy. The parameters are optimised through the genetic algorithm with an average optimisation time of 20 min offline. In addition, the muscle–tendon lengths of selected muscles are determined by the regression algorithm, including the complicated combination of the wrist movements with respect to wrist flexion/extension and radial/ulnar deviation. Other approaches to generate the subject-specific muscle–tendon model by scaling the model based on the recorded data, where the scaling process is not suitable for the amputees. To account for the subject-specificity, the scaling coefficient is introduced for the muscle–tendon length.

The tendon compliance could hurdle the real-time application of the musculoskeletal model-based approach, i.e., numerical stiffness in muscle–tendon model [41]. The tendon is assuming stiff enough in this study. The proposed model-based approach still guarantee accurate wrist joint angles estimation in response to the surface EMG signals. An average offline computation time of a 20 seconds trial is 0.556 seconds on a desktop computer with a quad-core processor and 32 GB RAM. It is indicated that the proposed model has the capability of real-time application.

4.3. Limitations and future work

The present study has several limitations. We evaluate the performance of the EMG-driven MSK model and the mirrored bilateral training strategy on a limited number of subjects. We will recruit more subjects, including amputated patients, to investigate the performance of the proposed MSK model and training strategy. Moreover, we do not design the experimental protocols with confounding scenarios. We will carry out to design more combinations of wrist motions and scenarios, e.g., different upper limb postures, to investigate the generalisation of the EMG-driven MSK model for myoelectric control. We do not compare the proposed MSK model with the model-free approaches, which should be studied in future work. Finally, future work will carry out to improve the parameter optimisation techniques to improve the subject-specificity of the EMG-driven MSK model.

5. Conclusion

In the present study, we proposed a MSK model to estimate the 2 DoFs of wrist kinematics of the contralateral limb based on the muscle activities from the ipsilateral limb using the mirrored bilateral movements. The proposed model interpreted the biological process from the muscle activities to wrist joint angles. In the contralateral case, the proposed approach shows that the mean R^2 are 0.86 and 0.82 for the wrist flexion/extension and radial/ulnar deviation respectively. Results indicate the potential solution for simultaneous and proportional control of wrist kinematics for the unilateral transradial amputee. Future works include the evaluation of the MSK model on the subjects and confounding scenarios and the comparison study with the model-free approaches.

CRediT authorship contribution statement

Yihui Zhao: Resources, Methodology, Writing – original draft, Writing – review & editing, Data curation, Conceptualization, Software. **Zhenhong Li:** Data curation, Writing – review & editing. **Zhiqiang Zhang:** Visualization, Writing – review. **Kun Qian:** Visualization, Writing – review. **Shengquan Xie:** Supervision.

Declaration of competing interest

The authors declare that they have no known competing financial interests or personal relationships that could have appeared to influence the work reported in this paper.

Data availability

No data was used for the research described in the article.

Acknowledgements

This work was supported in part by U.K. EPSRC under Grant EP/S019219/1 and Grant EP/V057782/1.

References

[1] L. Bi, C. Guan, et al., A review on EMG-based motor intention prediction of continuous human upper limb motion for human-robot collaboration, Biomed. Signal Process Control. 51 (2019) 113–127.
[2] C.G. McDonald, J.L. Sullivan, T.A. Dennis, M.K. O'Malley, A myoelectric control interface for upper-limb robotic rehabilitation following spinal cord injury, IEEE Trans. Neural Syst. Rehabilitation Eng. 28 (4) (2020) 978–987.
[3] M.B. Kristoffersen, A.W. Franzke, C.K. Van Der Sluis, A. Murgia, R.M. Bongers, Serious gaming to generate separated and consistent EMG patterns in pattern-recognition prosthesis control, Biomed. Signal Process. Control 62 (2020) 102140.
[4] A. Tigrini, L.A. Pettinari, F. Verdini, S. Fioretti, A. Mengarelli, Shoulder motion intention detection through myoelectric pattern recognition, IEEE Sens. Lett. 5 (8) (2021) 1–4.
[5] C. Piazza, M. Rossi, M.G. Catalano, A. Bicchi, L.J. Hargrove, Evaluation of a simultaneous myoelectric control strategy for a multi-dof transradial prosthesis, IEEE Trans. Neural Syst. Rehabilitation Eng. 28 (10) (2020) 2286–2295.
[6] J. Liu, Y. Ren, D. Xu, S.H. Kang, L.-Q. Zhang, EMG-based real-time linear-nonlinear cascade regression decoding of shoulder, elbow, and wrist movements in able-bodied persons and stroke survivors, IEEE. Trans. Biomed. 67 (5) (2019) 1272–1281.
[7] G. Gu, N. Zhang, H. Xu, S. Lin, Y. Yu, G. Chai, L. Ge, H. Yang, Q. Shao, X. Sheng, et al., A soft neuroprosthetic hand providing simultaneous myoelectric control and tactile feedback, Nat. Biomed. Eng. (2021) 1–10.
[8] P. Qin, X. Shi, A novel method for lower limb joint angle estimation based on sEMG signal, IEEE Trans. Instrum. Meas. 70 (2021) 1–9.
[9] D. Xiong, D. Zhang, X. Zhao, Y. Zhao, Deep learning for EMG-based human-machine interaction: a review, IEEE/CAA J. Autom. Sin. 8 (3) (2021) 512–533.
[10] Y. Yu, C. Chen, J. Zhao, X. Sheng, X. Zhu, Surface electromyography image-driven torque estimation of multi-DoF wrist movements, IEEE Trans. Ind. Electron. 69 (1) (2021) 795–804.
[11] Z. Lei, An upper limb movement estimation from electromyography by using BP neural network, Biomed. Signal Process Control 49 (2019) 434–439.
[12] T. Bao, S.A.R. Zaidi, S. Xie, P. Yang, Z.-Q. Zhang, A CNN-LSTM hybrid model for wrist kinematics estimation using surface electromyography, IEEE Trans. Instrum. Meas. 70 (2020) 1–9.
[13] L. Pan, D.L. Crouch, H. Huang, Comparing EMG-based human-machine interfaces for estimating continuous, coordinated movements, IEEE Trans. Neural Syst. Rehabilitation Eng. 27 (10) (2019) 2145–2154.
[14] L. Zhang, Z. Li, Y. Hu, C. Smith, E.M.G. Farewik, R. Wang, Ankle joint torque estimation using an EMG-driven neuromusculoskeletal model and an artificial neural network model, IEEE Trans. Autom. Sci. Eng. 18 (2) (2020) 564–573.
[15] Y. Sheng, J. Liu, Z. Zhou, H. Chen, H. Liu, Musculoskeletal joint angle estimation based on isokinetic motor coordination, IEEE Trans. Med. Robot. Bionics. 3 (4) (2021) 1011–1019.
[16] J. Han, Q. Ding, A. Xiong, X. Zhao, A state-space EMG model for the estimation of continuous joint movements, IEEE Trans. Ind. Electron. 62 (7) (2015) 4267–4275.
[17] D. Blana, E.K. Chadwick, A.J. van den Bogert, W.M. Murray, Real-time simulation of hand motion for prosthesis control, Comput. Methods Biomech. Biomed. Eng. 20 (5) (2017) 540–549.
[18] L. Pan, H.H. Huang, A robust model-based neural-machine interface across different loading weights applied at distal forearm, Biomed. Signal Process Control 67 (2021) 102509.
[19] Z. Zhu, C. Martinez-Luna, J. Li, B.E. McDonald, C. Dai, X. Huang, T.R. Farrell, E.A. Clancy, EMG-force and EMG-target models during force-varying bilateral hand-wrist contraction in able-bodied and limb-absent subjects, IEEE Trans. Neural Syst. Rehabilitation Eng. 28 (12) (2020) 3040–3050.
[20] I.J.R. Martínez, A. Mannini, F. Clemente, C. Cipriani, Online grasp force estimation from the transient EMG, IEEE Trans. Neural Syst. Rehabilitation Eng. 28 (10) (2020) 2333–2341.
[21] S. Oda, Motor control for bilateral muscular contractions in humans, Jpn.J.Physiol. 47 (6) (1997) 487–498.
[22] R.L. Lieber, B.M. Fazeli, M.J. Botte, Architecture of selected wrist flexor and extensor muscles, J. Hand Surg. Am. 15 (2) (1990) 244–250.
[23] N. Jiang, J.L. Vest-Nielsen, S. Muceli, D. Farina, EMG-based simultaneous and proportional estimation of wrist/hand kinematics in uni-lateral trans-radial amputees, J. Neuroeng. Rehabilitation 9 (1) (2012) 42.
[24] A. Kian, C. Pizzolato, M. Halaki, K. Ginn, D. Lloyd, D. Reed, D. Ackland, The effectiveness of EMG-driven neuromusculoskeletal model calibration is task dependent, J. Biomech. 129 (2021) 110698.
[25] D.G. Lloyd, T.F. Besier, An EMG-driven musculoskeletal model to estimate muscle forces and knee joint moments in vivo, J. Biomech. 36 (6) (2003) 765–776.
[26] T.S. Buchanan, D.G. Lloyd, K. Manal, T.F. Besier, Neuromusculoskeletal modeling: estimation of muscle forces and joint moments and movements from measurements of neural command, J. Appl. Biomech. 20 (4) (2004) 367–395.
[27] A. Seth, J.L. Hicks, T.K. Uchida, A. Habib, C.L. Dembia, J.J. Dunne, C.F. Ong, M.S. DeMers, A. Rajagopal, M. Millard, et al., OpenSim: Simulating musculoskeletal dynamics and neuromuscular control to study human and animal movement, PLoS Comput. Biol. 14 (7) (2018) e1006223.
[28] D. Martinez-Peon, E. Olguín-Díaz, A. Muñoz-Vázquez, P.C. Francisco, D.S. Méndez, Modeling and control of exoskeleton for wrist and forearm rehabilitation, Biomed. Signal Process Control 70 (2021) 103022.
[29] P. De Leva, Adjustments to Zatsiorsky-Seluyanov's segment inertia parameters, J. Biomech. 29 (9) (1996) 1223–1230.
[30] K. Park, P.-H. Chang, S.H. Kang, In vivo estimation of human forearm and wrist dynamic properties, IEEE Trans. Neural Syst. Rehabilitation Eng. 25 (5) (2016) 436–446.
[31] C.Y. Scovil, J.L. Ronsky, Sensitivity of a hill-based muscle model to perturbations in model parameters, J. Biomech. 39 (11) (2006) 2055–2063.
[32] J.L. Nielsen, S. Holmgaard, N. Jiang, K.B. Englehart, D. Farina, P.A. Parker, Simultaneous and proportional force estimation for multifunction myoelectric prostheses using mirrored bilateral training, IEEE. Trans. Biomed. 58 (3) (2010) 681–688.
[33] M.E. Gunduz, C.B. Pinto, F.G. Saleh Velez, D. Duarte, K. Pacheco-Barrios, F. Lopes, F. Fregni, Motor cortex reorganization in limb amputation: a systematic review of TMS motor mapping studies, Front. Neurosci. 14 (2020) 314.
[34] Q. Zhang, T. Pi, R. Liu, C. Xiong, Simultaneous and proportional estimation of multijoint kinematics from EMG signals for myocontrol of robotic hands, IEEE ASME Trans. Mechatron. 25 (4) (2020) 1953–1960.
[35] M. Sartori, J. Van De Riet, D. Farina, Estimation of phantom arm mechanics about four degrees of freedom after targeted muscle reinnervation, IEEE Trans. Med. Robot. Bionics. 1 (1) (2019) 58–64.
[36] T. Kapelner, M. Sartori, F. Negro, D. Farina, Neuro-musculoskeletal mapping for man-machine interfacing, Sci. Rep. 10 (1) (2020) 1–10.
[37] S. Muceli, D. Farina, Simultaneous and proportional estimation of hand kinematics from EMG during mirrored movements at multiple degrees-of-freedom, IEEE Trans. Neural Syst. Rehabilitation Eng. 20 (3) (2011) 371–378.
[38] K. Nizamis, N.H. Rijken, R. Van Middelaar, J. Neto, B.F. Koopman, M. Sartori, Characterization of forearm muscle activation in duchenne muscular dystrophy via high-density electromyography: a case study on the implications for myoelectric control, Front. Neurol. 11 (2020) 231.
[39] D. Ao, M.S. Shourijeh, C. Patten, B.J. Fregly, Evaluation of synergy extrapolation for predicting unmeasured muscle excitations from measured muscle synergies, Front. Comput. Neurosci. 14 (2020) 108.
[40] K. Veerkamp, W. Schallig, J. Harlaar, C. Pizzolato, C.P. Carty, D.G. Lloyd, M.M. van der Krogt, The effects of electromyography-assisted modelling in estimating musculotendon forces during gait in children with cerebral palsy, J. Biomech. 92 (2019) 45–53.
[41] M. Millard, T. Uchida, A. Seth, S.L. Delp, Flexing computational muscle: modeling and simulation of musculotendon dynamics, J. Biomech. Eng. 135 (2) (2013).